*Acta Oceanol. Sin.*, 2022, Vol. 41, No. 1, P. 11–20
https://doi.org/10.1007/s13131-021-1882-3
http://www.aosocean.com
E-mail: ocean2@hyxb.org.cn

# Submarine groundwater discharge and benthic biogeochemical zonation in the Huanghe River Estuary

Guangquan Chen[1, 2], Bochao Xu[3, 4*], Shibin Zhao[3, 4, 5], Disong Yang[3, 4, 5], William C. Burnett[6], Shaobo Diao[7], Maosheng Gao[7], Xingyong Xu[1, 2], Lisha Wang[3, 4, 5]

[1] Key Laboratory of Coastal Science and Integrated Management, First Institute of Oceanography, Ministry of Natural Resources, Qingdao 266061, China

[2] Laboratory for Marine Geology, Pilot National Laboratory for Marine Science and Technology (Qingdao), Qingdao 266237, China

[3] Frontiers Science Center for Deep Ocean Multispheres and Earth System/Key Laboratory of Marine Chemistry Theory and Technology of Ministry of Education, Ocean University of China, Qingdao 266100, China

[4] Marine Ecology and Environmental Science Laboratory, Pilot National Laboratory for Marine Science and Technology (Qingdao), Qingdao 266237, China

[5] College of Chemistry and Chemical Engineering, Ocean University of China, Qingdao 266100, China

[6] Department of Earth, Ocean and Atmospheric Science, Florida State University, Tallahassee 32306, USA

[7] Qingdao Institute of Marine Geology, China Geological Survey, Qingdao 266071, China

Received 26 January 2021; accepted 24 March 2021



**Abstract**

Submarine groundwater discharge (SGD) has received increasing attention by studies on coastal areas; however, its effects on biogeochemical zonation have not been investigated to date. The Huanghe River Estuary (HRE) is a world class river estuary with high turbidity, and heavy human regulation. This study investigated how SGD is related to the benthic biogeochemistry of the HRE. Based on the distribution of several parameters (e.g., salinity, temperature, dissolved oxygen (DO) levels, pH, radium isotopes, and nutrients), the HRE was subdivided into six different zones, and the SGD fluxes within each zone were quantified and compared. The highest SGD flux was found in the northwest nearshore zone, where it was more than one order of magnitude higher than in the offshore zone. High SGD resulted in low DO and pH, but high nutrient levels in the benthic boundary layer. The southeast nearshore zone was also characterized by high SGD flux, but benthic waters were more oxic because of the dominating inputs by the Huanghe River. These data suggest that such a zonation would help to understand benthic biogeochemical processes. High SGD may not only contribute to the estuarine nutrient budget, but may also contribute to the formation of hypoxia and acidification.

**Key words:** SGD zonation, benthic biogeochemistry, radium isotopes, Huanghe River Estuary

**Citation:** Chen Guangquan, Xu Bochao, Zhao Shibin, Yang Disong, Burnett C. William, Diao Shaobo, Gao Maosheng, Xu Xingyong, Wang Lisha. 2022. Submarine groundwater discharge and benthic biogeochemical zonation in the Huanghe River Estuary. Acta Oceanologica Sinica, 41(1): 11–20, doi: 10.1007/s13131-021-1882-3

## 1 Introduction

Over the past few decades, submarine groundwater discharge (SGD), including both recycled seawater and terrestrial fresh water, has received increasing attention from the scientific community. Most research has focused on the calculation of SGD fluxes, and showed that these are often very important compared with river discharge in both local case studies as well as global scale estimates (Burnett et al., 2006; Moore et al., 2008; Moore, 2010; Kwon et al., 2014). A recent estimate showed that even conservatively calculated SGD-derived nutrient fluxes matched the level of river contribution to the global ocean (Cho et al., 2018). It has been reported that SGD could alter the biogeochemical makeup of the ocean benthic boundary layer, with regard to aspects such as dissolved oxygen (DO) and pH, etc. For example, Santos and Eyre (2011) found that the water pH is inversely related to groundwater inputs as a result of acidic groundwater entering the estuary. Peterson et al. (2016) found that saline, cold, and anoxic groundwater generated a DO undersaturated bottom water mass, which provides a new perspective for understanding coastal hypoxia events. Therefore, SGD should be considered for both global ocean budgets and ecosystem management strategies to better understand the dynamic interactions at land-

Foundation item: The National Natural Science Foundation of China under contract Nos 41876075, 41706067 and 41620104001; the Basic Scientific Fund for National Public Research Institutes of China under contract No. 2017Q02; the Fundamental Research Funds for the Central Universities, China under contract Nos 201841007, 201962003 and 201762031; the Marine S&T Fund of Shandong Province for Pilot National Laboratory for Marine Science and Technology (Qingdao) under contract No. 2018SDKJ0503; the Youth Talent Support Program of the Laboratory for Marine Ecology and Environmental Science, Pilot National Laboratory for Marine Science and Technology (Qingdao) under contract No. LMEES-YTSP-2018-02-06.
*Corresponding author, E-mail: xubc@ouc.edu.cn

ocean interfaces.

The Huanghe River Estuary (HRE) is a world class major river estuary in China. SGD in the HRE has been found to be an important source of material, and thus, has to be considered in estuarine biogeochemical studies. SGD fluxes were found to be multiple times higher than the Huanghe River discharge during the same period, both by using seepage meters (Taniguchi et al., 2008) and radium/radon isotopes (Peterson et al., 2008; Xu et al., 2013, 2014; Wang et al., 2015, 2016; Xia et al., 2016). SGD-associated nutrients account for more than 70% of the total nutrient load of the HRE (Xu et al., 2013). It is commonly accepted that SGD dynamics are heterogenous in estuaries and coastal settings. Although SGD fluxes in the HRE have been well documented, a clear understanding of the zonation characteristics of the SGD dynamics in the HRE has still not been achieved. It remains unknown how SGD alters the biogeochemical characteristics of the benthic boundary layer of the HRE. In this study, radium isotopes in the HRE were applied as tracers to explore these scientific questions. By mapping the distributions of $^{224}$Ra, $^{223}$Ra, and $^{226}$Ra, combined with biogeochemical parameters (e.g., salinity, DO, pH, and nutrients), a zonation of the HRE is proposed based on the influences of SGD as well as that of the Huanghe River. SGD fluxes in each zone were calculated and compared to obtain a more detailed understanding of the biogeochemical influence that SGD imposes on the HRE.

## 2 Materials and methods

### 2.1 *Sampling and analytical methods*

One sampling cruise was conducted in the HRE in June 2014, which included 35 sampling stations as shown in Fig. 1. The Huanghe River discharge during the sampling period ranged from 214 m$^3$/s to 458 m$^3$/s (http://www.yrcc.gov.cn/), and salinity (in absolute salinity scale) in the study area ranged from 21.5 to 28.8. Surface and bottom water samples were collected for radium isotopes ($^{226}$Ra, $^{224}$Ra, and $^{223}$Ra) (Table S1) and nutrient (DIN, DIP, and DSi) analyses (Table S2) by sinking pump and conductivity-temperature-depth rosette. At each sampling station, salinity, temperature, pH, and DO were measured *in situ* by an XR-420 model submersible multichannel conductivity-temperature-depth sensor (RBR, Canada) (Table S2). During the same period, seven groundwater samples were collected along the coast of the Huanghe River Delta to obtain a groundwater endmember (Table S1). About 2 L of groundwater was collected at each site for radium analyses using a pushpoint sampler and a peristaltic pump. Known volumes of radium isotopes sample (80 L) were pre-concentrated by slowly passing through manganese impregnated acrylic fibers ("Mn-fibers") that quantitatively adsorbed dissolved radium. The average adsorption efficiency of these homemade fibers was evaluated in the laboratory to be 98%±2% (Xia et al., 2016). After collection, all fibers were thoroughly washed with Ra-free deionized water to remove any salt content and particulate matter, and then fibers were partially dried until the water/fiber mass ratio range reached 1–2 (Sun and Torgersen, 1998; Kim et al., 2001). The short-lived radium isotopes ($^{223}$Ra and $^{224}$Ra) were then counted via a radium delayed coincidence counting system (Moore and Arnold, 1996). Long-lived $^{226}$Ra was also measured by radium delayed coincidence counting following the procedure described by Waska et al. (2008). The analytical precisions for all three Ra isotopes exceeded 10%. More details about the water sampling and analysis have been reported previously by Xu et al. (2016) and Xia et al. (2016).

### 2.2 *Radium mass balance model for submarine groundwater discharge flux*

The SGD fluxes in the different zones of the HRE were calculated based on a mass balance model of $^{226}$Ra, assuming a steady state (Moore, 1996; Swarzenski, 2007). Given that the production of radium isotopes is governed by their decay constants, shallow recirculation of seawater through sediments, which occurs over short time scales (from hours to months), does not enable a significant ingrowth of the long-lived radium isotopes. Thus, sedimentary diffusion and radioactive decay of $^{226}$Ra ($t_{1/2}$ =1 600 a) were negligible in this model (Moore, 2007; Rodellas et al., 2017). The excess $^{226}$Ra flux can thus be converted to SGD flux (cm/d) as

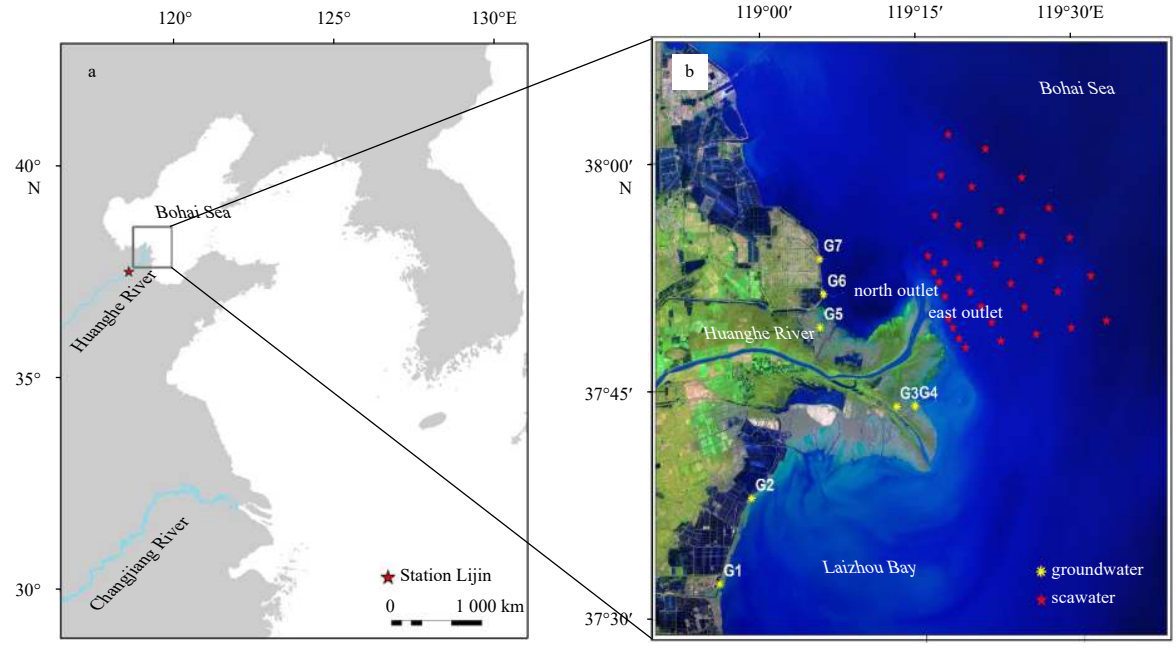


**Fig. 1.** Study area of the Huanghe River Estuary (a), and locations of sampling stations for seawater and groundwater in June 2014 (b).

following:

$$\mathrm{SGD} = \frac{(A - A_o)\cdot z/\tau - (A_r Q_r + A_d C_{spm} Q_r)/S}{A_{gw}} \times 100, \quad (1)$$

where $A$, $A_o$, and $A_{gw}$ represent $^{226}$Ra activities (Bq/m$^3$) in coastal water, offshore seawater, and groundwater endmembers, respectively. The parameters $z$ and $S$ represent the average water depth (m) and the area of the individual zones (m$^2$), respectively. The term $\tau$ represents the water residence time (d). $A_r$ represents the dissolved $^{226}$Ra concentration (Bq/m$^3$) in the Huanghe River. $A_d$ represents the desorbed radium from suspended particles (Bq/g). $C_{spm}$ represents the concentration of suspended particulate matter in the Huanghe River (g/m$^3$). Finally, $Q_r$ represents the Huanghe River discharge (m$^3$/d).

### 2.3 *Water residence time model*

Moore et al. (2006) proposed a general water age model that combines two radium mass balance models including radium sources from sediments, rivers, SGD, and sinks caused by the mixing and decay losses at the Okatee Estuary, where SGD and decay are the major terms in the mass balance model. While in area of the HRE, the inputs of radium included SGD, benthic diffusion, rivers, and sedimentary inputs. Thus, the water residence time was calculated based on the improved radium water age model according to Zhang et al. (2020) and Wang et al. (2020) as following:

$$\tau = \frac{F_{^{224}\mathrm{Ra}/^{226}\mathrm{Ra}} \times (I_{^{226}\mathrm{Ra}} - V\cdot A_{\text{o-}^{226}\mathrm{Ra}}) - (I_{^{224}\mathrm{Ra}} - V\cdot A_{\text{o-}^{224}\mathrm{Ra}})}{(\lambda_{^{224}\mathrm{Ra}}\cdot I_{^{224}\mathrm{Ra}} - F_{\text{r-}^{224}\mathrm{Ra}} - F_{\text{sed-}^{224}\mathrm{Ra}}) - F_{^{224}\mathrm{Ra}/^{226}\mathrm{Ra}}\cdot(\lambda_{^{226}\mathrm{Ra}}\cdot I_{^{226}\mathrm{Ra}} - F_{\text{r-}^{226}\mathrm{Ra}} - F_{\text{sed-}^{226}\mathrm{Ra}})}, \quad (2)$$

where $F_{^{224}\mathrm{Ra}/^{226}\mathrm{Ra}}$ represents the $^{224}$Ra/$^{226}$Ra activity ratio (AR) of the flux into the system; $I$, the inventory (Bq) of Ra in the study area; $V$, the water volume (m$^3$) in the study area; and $F_r$ and $F_{sed}$ represent the Ra inputs (Bq/d) from rivers and sediments.

### 2.4 *Three-end-members mixing model for the river water fraction*

A three-end-members mixing model was used to estimate the fractions of water from three different endmembers (Moore et al., 2006), which are ocean, river, and groundwater. The $^{226}$Ra balance equations are as following:

$$f_o + f_r + f_{gw} = 1, \quad (3)$$

$$\left[^{226}\mathrm{Ra}_o\right] f_o + \left[^{226}\mathrm{Ra}_r\right] f_r + \left[^{226}\mathrm{Ra}_{gw}\right] f_{gw} = \left[^{226}\mathrm{Ra}_{obs}\right], \quad (4)$$

$$S_o f_o + S_r f_r + S_{gw} f_{gw} = S_{obs}, \quad (5)$$

where $f$ represents the fraction of each endmember; [Ra], the concentration of radium isotopes; $S$, the value of salinity; the subscript o, r, gw, and obs, imply samples from the ocean, the Huanghe River, groundwater, and observation stations, respectively.

The fraction of the Huanghe River can be calculated by the following equation:

$$f_r = \frac{\left(\frac{\left[^{226}\mathrm{Ra}_{obs}\right] - \left[^{226}\mathrm{Ra}_o\right]}{\left[^{226}\mathrm{Ra}_{gw}\right] - \left[^{226}\mathrm{Ra}_o\right]}\right) - \left(\frac{S_{obs} - S_o}{S_{gw} - S_o}\right)}{\left(\frac{\left[^{226}\mathrm{Ra}_r\right] - \left[^{226}\mathrm{Ra}_o\right]}{\left[^{226}\mathrm{Ra}_{gw}\right] - \left[^{226}\mathrm{Ra}_o\right]}\right) - \left(\frac{S_r - S_o}{S_{gw} - S_o}\right)}. \quad (6)$$

## 3 Results

### 3.1 *Biogeochemical zonation characteristics in the benthic HRE*

The distribution patterns of all measured parameters within the benthic layer are shown in Fig. 2. The biogeochemical characteristics in different regions of the benthic HRE differed strongly during the investigation. Because the water depth in the southeast of the HRE was about 1 m shallower than in the northwest region, the Huanghe River water would more easily flow toward the southeast direction after leaving the river mouth. This also agrees with previous observations via satellite images, which indicated that in the river mouth region, the Huanghe River flowed a short distance northward and was then directed to a more southeastern direction by the prevailing currents (Xu et al., 2016). Therefore, the bottom water in the southeast region was more influenced by the river, with lower salinity (Fig. 2a) and higher temperature (Fig. 2b). Because of strong mixing throughout the water column of the southeast region, DO, pH, and benthic turbidity were all higher than in the northwest region (Figs 2c-e), demonstrating stronger influences by the Huanghe River. The highest concentrations of all three radium isotopes were found in the nearshore northwest region of the benthic HRE (Figs 2f-h). Here, nutrient concentrations (especially DIN and DSi) were also highest (Figs 2i-k), while DO and pH were lowest (Figs 2d and e). Since the Huanghe River diluted water was not actively flushing this region, and since the benthic turbidity was low, the only reason for the higher radium concentrations would be SGD. Since groundwater is usually anoxic and somewhat acidic, significant groundwater discharge would result in lower DO and pH in the benthic layer. Therefore, these observations identified SGD as an important contributor to benthic HRE biogeochemistry.

Based on the measured benthic biogeochemical characteristics, the HRE was subsectioned into two major regions (Fig. 3): (1) the northwest region, which was more significantly influenced by SGD; and (2) the southeast region, which was dominated by the Huanghe River. To arrive at a more detailed comparison, each region was further divided into three zones based on distance from nearshore to offshore. Zone I was characterized by the shallowest water depth, the highest radium and nutrient levels, but the lowest DO and pH levels. The sediment particle sizes within Zone I of both regions were coarser, especially near the two river outlets (either sand or clay sand, Figs 4a and b). After the initiation of the Water Sediment Regulation Scheme (WSRS) in 2013, a new river delta appeared at the Huanghe River mouth, leading to the formation of two river outlets (north outlet and east outlet; Fig. 1) and resulting in a double-plume distribution pattern (Xu et al., 2016). At the junction of these two regions, however, the sediment was mainly composed of clay (exceeding 30%). Zone II was more like a transition zone, where the DO and pH were low, and radium isotopes and nutrients were not as high as in Zone I. Zone III had the deepest water, lowest radium isotopes and nutrient levels, and higher DO and pH levels. Sediment was sand in the

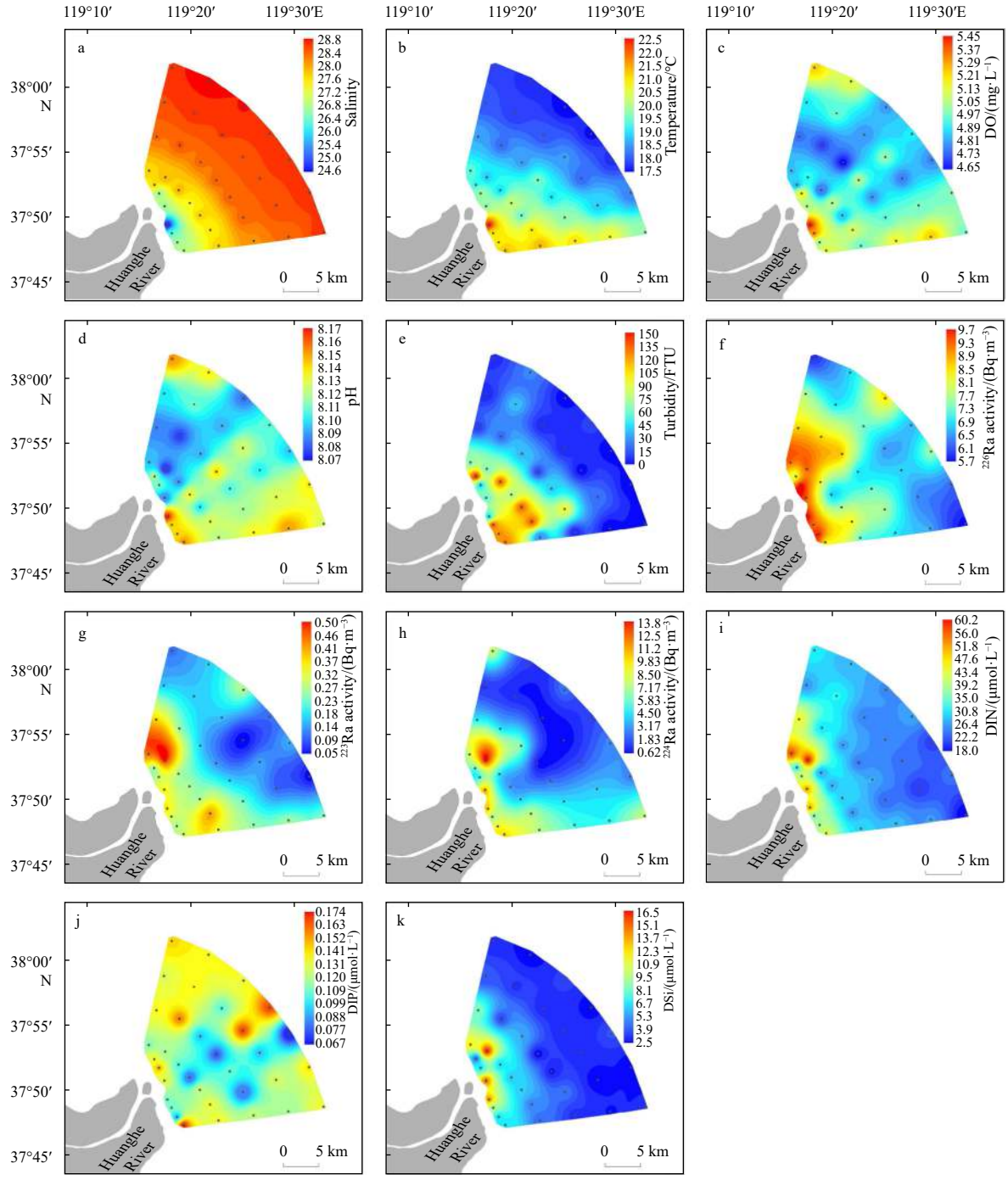


**Fig. 2.** Distribution of hydrological parameters (a–e), radium isotopes activities (f–h), and nutrients (i–k) in the Huanghe River Estuary in June 2014.

northwest region, and clay in the southeast region (Figs 4a and c).

### 3.2 *Submarine groundwater discharge fluxes in different zones of the Huanghe River Estuary*

The SGD flux was estimated based on a mass balance model of $^{226}$Ra. Equation (1) was applied to calculate the SGD fluxes within six different zones of the HRE. All required parameters are listed in Table 1. The average coastal $^{226}$Ra concentrations ($A$) were the averages of the surface and bottom radium concentrations at each sampling station. Based on the geometry of each region and zone, the $S$ and $V$ for each compartment were estimated. The $A_o$ was the lowest $^{226}$Ra concentration (2.73±0.08) Bq/m$^3$ identified during the expedition. This estimate is very close to the documented seawater $^{226}$Ra in the HRE (2.1 Bq/m$^3$; Xia et al., 2016), as well as the concentrations in the Bohai Sea and the north Yellow Sea ((3.07±0.81) Bq/m$^3$; Wang et al., 2010). The oceanic Ra fluxes contribute about 30%–40% to the total estuarine Ra fluxes in each zone (Table 1).

Water residence times were calculated based on the improved water age model via Eq. (2). The highest observed $^{224}$Ra/$^{226}$Ra ratio was chosen as the endmember value, which initially flushed into the system, and which was 1.5 in the north

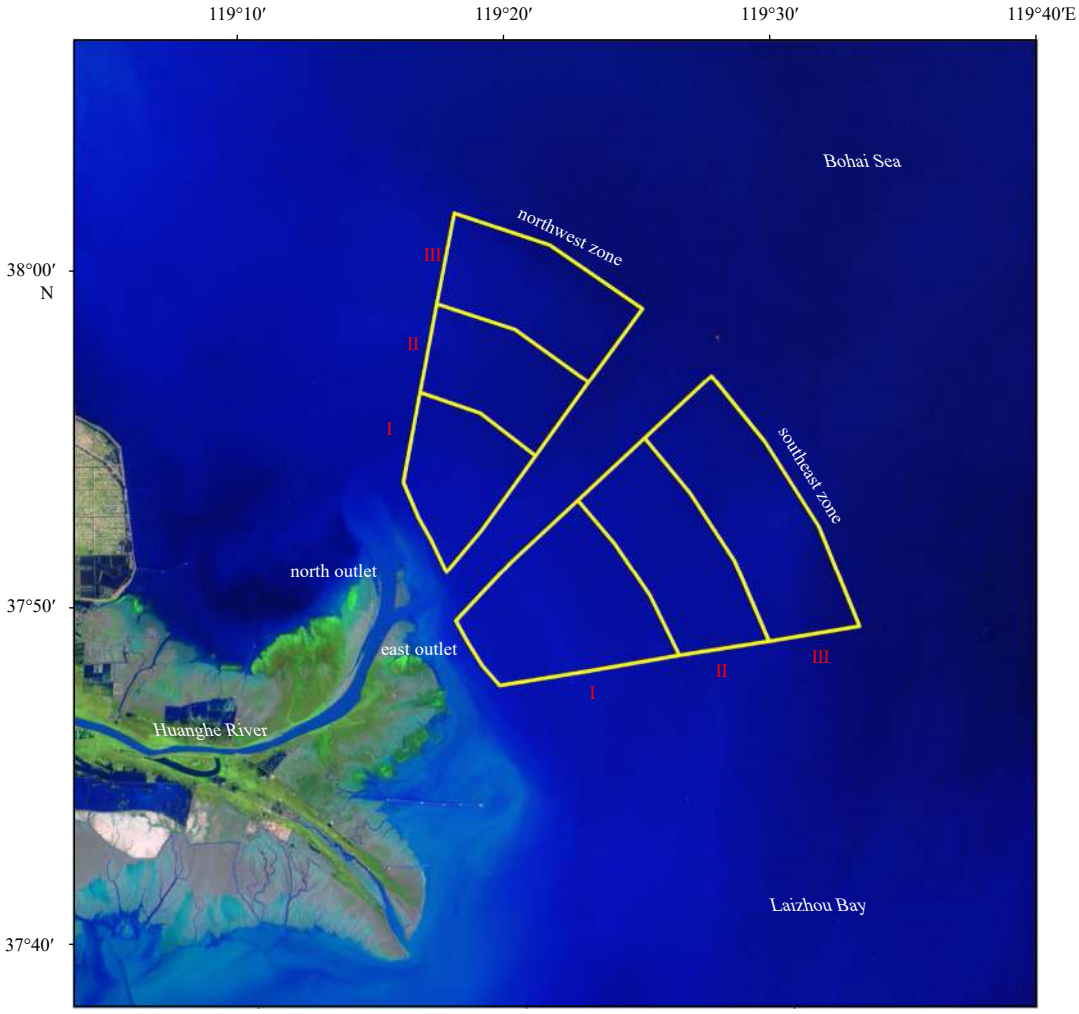


**Fig. 3.** Sketched zonation characteristics.

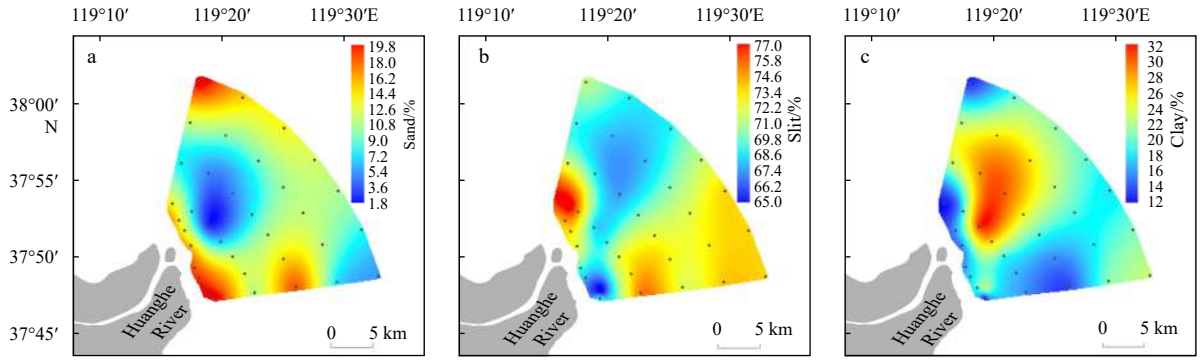


**Fig. 4.** Percentage distributions of different particle size sediments. Sediment type was determined by the median particle size, the ranges of which were –1Φ–4Φ, 4Φ–8Φ, and >8Φ for sand, slit, and clay, respectively.

zone and 1.3 in the south zone, respectively. The inventory of $^{224}$Ra and $^{226}$Ra in the estuary was determined by the triangular irregular networks method, with a spatial resolution of 100 m× 100 m. The ocean endmember of $^{224}$Ra and $^{226}$Ra was determined by the minimum value in each zonation. Radium input from river included the dissolved radium concentration in the Huanghe River and the desorbed radium from suspended particles is shown in Table 1. Radium input from sediments is mainly caused by short-lived isotopes from fine-grained sediments, hence, the fluxes of $^{224}$Ra from fine-grained sediments in this study were used a value of 3.5 Bq/(m$^2$·d) (Moore, 2007). This value was also employed by Wang et al. (2016) in their research on the HRE. The water ages estimated by $^{224}$Ra and $^{226}$Ra are showed in Table 1. Although the area in the southeast region was twice as large as that of the northwest region, the water residence time was about 36% shorter, demonstrating that the estuarine plume was mainly flushing toward the southeast direction.

The river contribution in each subarea of the HRE was calcu-

**Table 1.** Measured and derived parameters for a $^{226}$Ra mass balance model to assess submarine groundwater discharge (SGD)

| Parameters | Northwest region | | | Southeast region | | |
|---|---|---|---|---|---|---|
| | Zone I | Zone I+II | Zone I+II+III | Zone I | Zone I+II | Zone I+II+III |
| $A$/(Bq·m$^{-3}$) | 8.28±0.23 | 7.97±0.22 | 7.53±0.22 | 7.78±0.22 | 7.48±0.20 | 7.23±0.20 |
| $z$/m | 9.8 | 11.4 | 12.5 | 10.2 | 11.7 | 12.8 |
| $S$/km$^2$ | 39.8 | 82 | 134 | 71 | 128 | 200 |
| $V$/(10$^9$ m$^3$) | 0.5 | 1.1 | 2.0 | 0.8 | 1.7 | 2.9 |
| $\tau$/d | 5.5±1.0 | 8.6±1.7 | 13.6±2.6 | 4.7±1.0 | 7.8±1.5 | 10.2±1.9 |
| Estuarine Ra flux=($A\times V/\tau$)/(10$^9$ Bq·d$^{-1}$) | 0.78 | 0.94 | 1.08 | 1.30 | 1.77 | 2.09 |
| $A_o$/(Bq·m$^{-3}$) | 2.73±0.08 | 2.73±0.08 | 2.73±0.08 | 2.73±0.08 | 2.73±0.08 | 2.73±0.08 |
| Oceanic Ra flux=($A_o\times V/\tau$)/(10$^9$ Bq·d$^{-1}$) | 0.26 | 0.33 | 0.39 | 0.46 | 0.65 | 0.79 |
| $Q_r$/(10$^7$ m$^3$·d$^{-1}$) | 3.3 | 3.3 | 3.3 | 3.3 | 3.3 | 3.3 |
| $A_r$/(Bq·m$^{-3}$) | 4.47±0.12 | 4.47±0.12 | 4.47±0.12 | 4.47±0.12 | 4.47±0.12 | 4.47±0.12 |
| Oceanic Ra contribution/% | 22 | 20 | 20 | 78 | 80 | 80 |
| Riverine dissolved Ra flux=($A_r\times Q_r$)/(10$^8$ Bq·d$^{-1}$) | 0.33 | 0.30 | 0.30 | 1.15 | 1.18 | 1.18 |
| $C_{spm}$/(g·m$^{-3}$) | 252 | 252 | 252 | 252 | 252 | 252 |
| $A_d$/(Bq·g$^{-1}$) | 1.33 | 1.33 | 1.33 | 1.33 | 1.33 | 1.33 |
| Riverine dissolved Ra contribution/% | 21 | 22 | 22 | 79 | 78 | 78 |
| Riverine Ra flux=($A_d\times C_{spm}\times Q_r$)/(10$^6$ Bq·d$^{-1}$) | 1.83 | 1.66 | 1.66 | 6.49 | 6.65 | 6.65 |
| $A_{gw}$/(Bq·m$^{-3}$) | 11.25±0.58 | 11.25±0.58 | 11.25±0.58 | 27.38±1.32 | 27.38±1.32 | 27.38±1.32 |
| $F_{SGD}$/(cm·d$^{-1}$) | 97±20 | 68±15 | 44±9 | 38±14 | 26±8 | 21±6 |
| $S\times F_{SGD}$/ (10$^7$ m$^3$·d$^{-1}$) | 3.9±0.8 | 5.6±1.2 | 5.9±1.2 | 2.7±1.0 | 3.3±1.0 | 4.2±1.2 |
| | Zone I | Zone II | Zone III | Zone I | Zone II | Zone III |
| $F_{SGD}$ in each zone=[($F_{SGD}$ $S$)$_{i+1}$– ($F_{SGD}$ $S$)$_i$]/ ( $S_{i+1}$ – $S_i$)/(cm·d$^{-1}$) | 97±20 | 39±35 | 7±33 | 38±14 | 11±27 | 12±29 |

Note: Water ages ($\tau$) were calculated based on Eq. (2). The contribution of the river was calculated based on Eqs (3)–(6). The radium desorption coefficient ($A_d$) was based on lab experiments at a salinity of 30 (Yang et al., 2019). Areas ($S$) were estimated based on the geometry of each study area. $F_{SGD}$ in Zone II and Zone III were calculated based on the differences of SGD fluxes in Zone I, Zone I+II, and Zone I+II+III. $i$ represents Zone I, Zone II or Zone III (ie., when $i$ represents Zone I, $i$+1 implies Zone II, by analogy).

lated based on the three-end-members model. The radium endmembers of ocean, river, and groundwater in this model are listed in Table 1. The salinity endmembers of ocean and river were defined as 28.8 and 0.4, and the groundwater was defined as 26.7 in the north and 31.7 in the south based on the field data. The calculation results show that river discharge mainly happened in the southeast region (78%–80%), which agrees with the results of water ages.

The riverine $^{226}$Ra flux was derived from a combination of river water dissolved radium and the radium desorbed from suspended particles. The concentrations of dissolved $^{226}$Ra and suspended particles in the Huanghe River ($A_r$) were 4.47 Bq/m$^3$ and 252 g/m$^3$ based on samples collected at the Station Lijin (Fig. 1). Station Lijin is located about 100 km upstream of the river mouth and has near zero salinity. The desorbed $^{226}$Ra from suspended particles ($A_d$) was estimated to be 1.33 Bq/g, based on laboratory simulation experiments at a salinity of 30 with different suspended particle concentration scenarios (Yang et al., 2019). This value is one order of magnitude lower than a previous rough estimate based on the difference of $^{226}$Ra activities in river suspended particles and estuarine bottom sediments (Peterson et al., 2008). The riverine Ra flux only contributed 4%–8% to the total Ra in the HRE, most of which originated from the dissolved form in the Huanghe River. Therefore, even if the desorption coefficient increased by an order of magnitude, the river particulate desorption Ra flux would still be negligible, and would not change the overall riverine Ra fluxes as part of the total estuarine Ra budget.

The $^{226}$Ra activity in the groundwater endmember was based on an average of seven samples collected along the Huanghe River Delta coastal line. All samples consisted of saline groundwater with salinities of 23–42. The $^{226}$Ra concentrations ranged from 10.5 Bq/m$^3$ to 36.5 Bq/m$^3$. To appropriately calculate the SGD flux in each zone, the groundwater endmember was divided into two parts, demarcated by the Huanghe River (Fig. 1). The groundwater endmember of north-west zone consists of G5 to G7, which average $^{226}$Ra concentrations of (11.25±0.58) Bq/m$^3$, while the south-east groundwater endmember consists of G1 to G4 with average $^{226}$Ra concentrations of (27.38±1.32) Bq/m$^3$.

The SGD fluxes in the two major regions (northwest region and southeast region) were 44 cm/d and 21 cm/d, respectively. The SGD flux through the northwest region was twice of that of the southeast region. Furthermore, if SGD fluxes are compared within the subsections of these two major regions, the differences become much more profound. Considering the individual compartments of the two regions, SGD fluxes decreased progressively along the offshore direction. The highest SGD flux (97 cm/d) was found in the most nearshore area, i.e., Zone I of the northwest region. The lowest SGD flux (7 cm/d) was found in Zone III of the northwest region, which was less than 10% of that in Zone I. The fluxes in Zone II of the northwest region and Zone I of the southeast region ranged between the extremes and were very similar to each other (~38 cm/d). They were only about one third of the SGD flux in Zone I of the northwest region. The fluxes in Zone II and III (~11 cm/d) were slightly higher than in Zone III in the northwest region, but still at the lower end. Intense groundwater discharge in the Zone I of the northwest region could be a significant factor leading to the hypoxic and acidfied benthic characteristics. This is very different to the other zones of the HRE.

### 3.3 *Uncertainty analysis of submarine groundwater discharge in the Huanghe River Estuary*

A box model of mass balance was built to calculate SGD fluxes in the HRE, where the radium removal processes (i.e.,

sinks) include loss via radioactive decay and mixing with the open sea water, while the sources include input from groundwater and river, as well as diffusion from sediments. The uncertainty of SGD in the HRE consisted of the propagation of counting errors and the uncertainties in water age, as well as fresh and seawater endmembers. Based on Eq. (2), the uncertainties in water age estimation are mainly associated with the terms of input ratio of $^{224}Ra/^{226}Ra$ and the inventories of $^{224}Ra$ and $^{226}Ra$. The input ratio of $^{224}Ra/^{226}Ra$ was based on the maximum ratio in the system, and the inventory of $^{224}Ra$ and $^{226}Ra$ was calculated by triangular irregular networks, with a spatial resolution of 100 m× 100 m. A variation of 1 d would cause changes of 20%–30%, 10%–18%, and 7%–12% in SGD flux in Zone I, Zone II, and Zone III, respectively. The water age in each zone has a standard deviation of 1–2.7 d, which yielded no more than 30% changes in SGD flux estimations.

More than 55% of the radium in estuaries originates from the contribution of groundwater inputs; therefore, variations in the estimated groundwater endmember value lead to the highest uncertainty of the SGD estimations. In general, radium is usually enriched in brackish groundwater relative to fresh groundwater (Mulligan and Charette, 2006), particularly long-lived isotopes. The groundwater endmember in this case consisted of saline groundwater with salinities of 23–42, which reached the maximum desorption of radium in brackish water. $^{226}Ra$ activities in groundwater ranged from 18.8 Bq/m$^3$ to 36.6 Bq/m$^3$ in the north of the HRE and 10.5 Bq/m$^3$ to 12.2 Bq/m$^3$ in the south of HRE, and the difference between both was significant. The groundwater endmember chosen in previous studies was 9.5 Bq/m$^3$ (Peterson et al., 2008; Xia et al., 2016), whereas both samples were collected in the south of the HER. Considering that the short-lived radium isotopes exhibit the same trend, the groundwater evolution process in these two areas is likely different. Therefore, two different groundwater endmembers were chosen in this area. In addition, the uncertainties emerging from the groundwater endmember were the propagation of counting errors during the calculation of averages, which caused a change of 4.8%–5.2% in SGD flux. The oceanic radium fluxes contribute about 30%–40% to the total estuarine radium fluxes, and the uncertainty of SGD flux estimates caused by seawater endmember was 2%. The riverine radium flux only contributed 4%–8% of the total radium in the HRE, which caused a change of 0.1%–0.2% in SGD flux. Therefore, uncertainties in fresh and seawater endmembers did not contribute significantly to the overall uncertainty.

The largest uncertainties in SGD flux estimates originate from the propagation of counting errors of the SGD flux calculation in Zone II and Zone III. The uncertainties resulting from subtraction between Zone$_i$ and Zone$_{i+1}$ were nearly ±300%. The statistical differences of SGD fluxes in Zone II and Zone III were not significant. However, even considering these uncertainties, the magnitude of SGD fluxes in Zone I is still significantly higher than that of Zone II and Zone III.

## 4 Discussion

### 4.1 *A synthesized view of submarine groundwater discharge in the Huanghe River Estuary*

Studies on SGD processes and their associated ecological influences in the HRE have been conducted for about two decades. At the beginning of the 21st Century, researchers used a hydrological model to quantify fluxes of terrestrial (i.e., fresh) groundwater discharge, which was found to be less than 0.01% of the total Huanghe River discharge (Qiu et al., 2003). However, the modern broad definition of SGD includes both a terrestrial fresh component (FSGD) and a recirculated seawater component (RSGD) (Burnett et al., 2003; Moore, 2010). Following this approach, other researchers started to evaluate the total SGD in the HRE and the coastal area of the Huanghe River Delta, and found much larger SGD fluxes on both a very local scale (within few kilometers offshore) (Peterson et al., 2008; Xia et al., 2016) as well as on a regional scale (up to thousands square kilometers) (Xu et al., 2013; Wang et al., 2015, 2016; Zhang et al., 2018). The recent estimates exceed the Huanghe River discharge. In this study, the total SGD flux for the whole study area was estimated as $1.01\times10^8$ m$^3$/d ($\sum_{i=1}^{3} F_{SGD}\times S_i$ in Table 1), which is three times higher than the Huanghe River discharge ($3.3\times10^7$ m$^3$/d).

Compared with the results of other areas, the SGD flux in the HRE is clearly at the upper end. Based on recent syntheses by Liu et al. (2017) and Wang et al. (2018), SGD fluxes in most marginal seas ranged from 0.01 cm/d to 155 cm/d, and most values were less than 5 cm/d. The SGD fluxes in the HRE have been calculated to be in the range 2–136 cm/d (Table 2). During periods when the Huanghe River had higher river discharge, the SGD flux would increase dramatically. The WSRS is an annual water-sediment management event, when the Huanghe River discharge was intentionally increased to more than one order of magnitude higher compared with the normal condition (implying increases from hundreds cubic meter per second to thousands cubic meter per second within a few days, which lasted for about 2 weeks every year). Xia et al. (2016) reported increases of the SGD flux from 2–20 cm/d to 67–122 cm/d during the WSRS event.

Recirculated seawater is clearly the dominant SGD component in the HRE and adjacent sea. Radium mainly accumulates in saline groundwater, while radon is normally enriched in all types of groundwater. Thus, the difference between the radium (RSGD) and radon (total SGD) models for calculated SGD fluxes would be a measure of the fresh component (FSGD). Based on this principle, the FSGD component was found to contribute less than 10% to the total SGD under normal river hydrodynamic conditions (Wang et al., 2015; Xia et al., 2016; Zhang et al., 2018).

**Table 2.** Comparison of SGD fluxes in Huanghe River Estuary

| Research region | Year | SGD/(cm·d$^{-1}$) | Approach | Reference |
|---|---|---|---|---|
| Huanghe River Estuary | 2004–2006 | 3.3–130.0 | seepage meters | Taniguchi et al. (2008) |
| | 2006–2007 | 4.5–24.2 | $^{223}Ra$, $^{224}Ra$, $^{226}Ra$, and $^{222}Rn$ | Peterson et al. (2008) |
| | 2010 | 13–136 | $^{226}Ra$ | Xu et al. (2013) |
| | 2012–2013 | 2–122 | $^{226}Ra$ and $^{222}Rn$ | Xia et al. (2016) |
| | 2014 | 7–98 | $^{224}Ra$ and $^{226}Ra$ | this study |
| Laizhou Bay | 2012 | 8.9–10.3 | $^{223}Ra$ and $^{226}Ra$ | Wang et al. (2015) |
| | 2012 | 7 | $^{224}Ra$ | Wang et al. (2016) |
| | 2014 | 10.2–15.0 | $^{223}Ra$, $^{224}Ra$, $^{226}Ra$, and $^{222}Rn$ | Zhang et al. (2018) |

However, during a WSRS event, the FSGD contribution increased to more than 20% of the total SGD, especially in the river mouth area where the FSGD component increased up to 40% (Xia et al., 2016). This relatively fresh benthic discharge was apparently sufficiently strong to disturb the benthic hyperpycnal flows, leading to very abrupt variations in bottom water dissolved oxygen and turbidity profiles (Xu et al., 2014).

The SGD distribution patterns in the HRE were found to be very heterogeneous both spatially and temporally. In this study, the SGD flux in the Zone I of the northwest region was found to be more than one order of magnitude higher than that in the Zone III of both northwest and the southeast regions. Previously, using automated seepage meters, Taniguchi et al. (2008) documented the highest SGD flux (of up to 130 cm/d) in an area about 3 km offshore, where it was about one order of magnitude higher than in both nearshore and offshore directions. During a WSRS, Xia et al. (2016) reported an even more dramatic difference with the highest fluxes near the Huanghe River mouth at more than 20 times higher than the lowest flux offshore.

### 4.2 *Submarine groundwater discharge vs. pore water exchange in the Huanghe River Estuary*

SGD has been recognized as an important source term for nutrients in the HRE. Peterson et al. (2008) reported that the SGD input nitrate flux was 2–3 times higher than that delivered by the Huanghe River. This may help to understand the increasing DIN levels in the central Bohai Sea over the past few decades. Xu et al. (2013) reported that the SGD associated nutrients contributed more than 70% of all the estuarine nutrient sources. During WSRS events, the increased SGD significantly enhanced nutrient fluxes (Xu et al., 2014). However, these nutrient fluxes were calculated by simply multiplying the dissolved nutrient concentrations in the groundwater endmember by the SGD flux. These nutrient fluxes have to be interpreted with care, because geochemical reactions often alter the nutrient behavior within subterranean estuaries and in the benthic water-sediment boundary layer before discharge (Kroeger and Charette, 2008; Young, 2013).

In addition to nutrients, SGD may alter the biogeochemical profile of the benthic HRE in other aspects, such as DO and pH. A recent study showed that radium-traced high SGD flux areas overlapped geographically with the hypoxia zone off the Changjiang River Estuary, indicating that SGD is highly possibly an important contributor to the seasonal coastal hypoxia formation (Guo et al., 2020). Considering that the south region of the HRE was significantly influenced by the Huanghe River, the present study only explored the SGD contribution to DO and pH variations in the northern region. As shown in Fig. 5, the DO and pH levels were negatively correlated with SGD fluxes. As the most significant SGD area, Zone I in the northwest region had the lowest DO and pH (Fig. 5). Most groundwaters are anoxic and acidic with low DO and pH (Kroeger and Charette, 2008; Santos and Eyre, 2011; Peterson et al., 2016). Intense groundwater discharge may thus directly decrease benthic DO and pH levels. Moreover, since reductive materials (e.g., U (IV), $Fe^{2+}$, $Mn^{2+}$, $H_2S$, and $NH_4^+$) may be concentrated in the aquifer (Slomp and Van Cappellen, 2004; Charette and Sholkovitz, 2006; Moore, 2010; Null et al., 2011; O'Connor et al., 2018), components in the recharging oxic seawater may be reduced and the fluids may become anoxic/hypoxic when discharged as RSGD. Since SGD-associated nutrients may trigger phytoplankton blooms, subsequent organic matter decomposition could also stimulate DO consumption and $H^+$ production. It is therefore reasonable to speculate that significant SGD within an estuarine environment may be an important contributor to the formation of coastal hypoxia and acidification.

Pore water exchange (PEX) driven by bioturbation, bioirrigation, shear flow, or flow-topography interactions has been identified as ubiquitous in the coastal sea and has been shown to enhance the fluxes of dissolved compounds to overlying waters

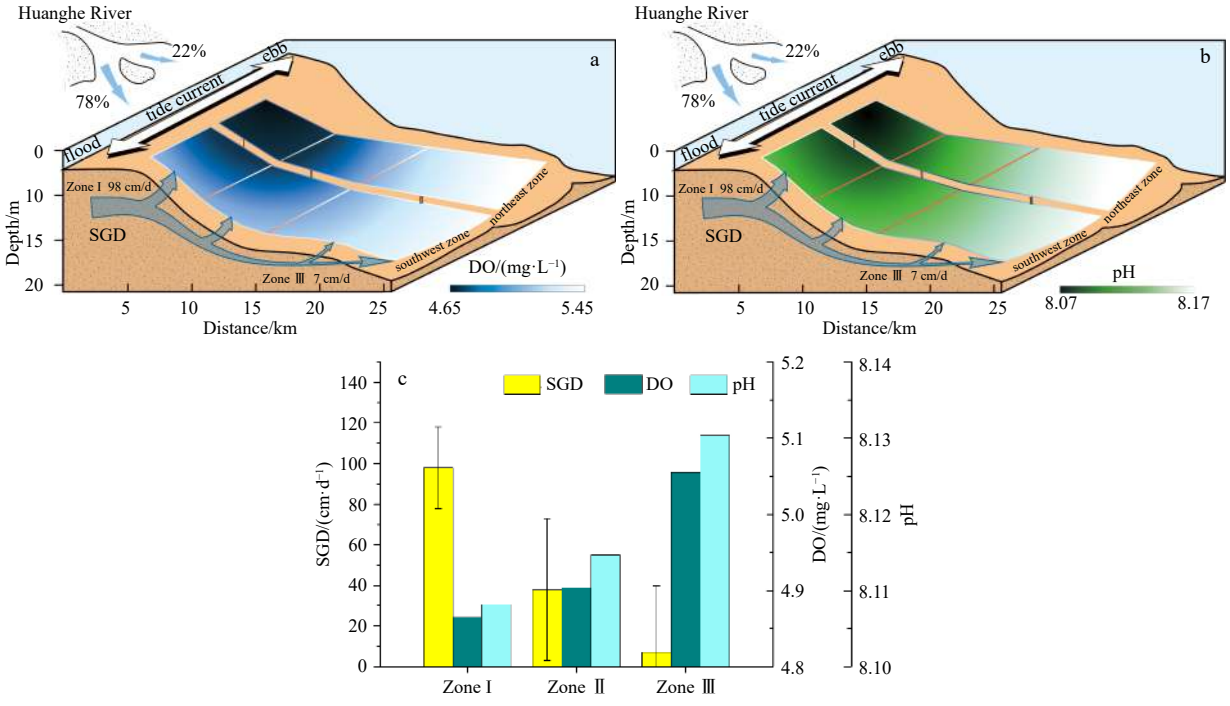


**Fig. 5.** Diagram illustrating the modes of submarine groundwater discharge (SGD) flux, dissolved oxygen (DO) (a) and pH (b) in the Huanghe River Estuary (HRE). Average SGD fluxes, DO and pH in bottom waters in the north HRE (c).

(based on $^{224}Ra/^{228}Th$ disequilibrium in sediments pioneered by Cai et al. (2014, 2015, 2020). Seawater entering the sediments carries oxygen and organic matter, both of which fuel biogeochemical reactions within sediments, resulting in the high enrichment of pore fluids in many dissolved constituents relative to overlying waters (mainly dissolved inorganic carbon, nutrients, and trace metals) (Huettel and Rusch, 2000; Rao et al., 2012; Rodellas et al., 2017; Shi et al., 2019). Notably, Shi et al. (2019) constructed a $^{224}Ra/^{228}Th$ disequilibrium approach to estimate benthic fluxes of $^{224}Ra$ induced by PEX into the coastal China seas, including one station near the HRE. Their results showed that $^{224}Ra$ fluxes were 20.33 Bq/($m^2$·d), which could be converted to $2.72\times10^9$ Bq/d in the northern region of the HRE and to $4.07\times10^9$ Bq/d in the southern region of the HRE. Based on Eq. (1), SGD fluxes into the Huanghe River Estuary were estimated to be $5.9\times10^7$ $m^3$/d and $4.2\times10^7$ $m^3$/d in the northern region and southern region, respectively. Combined with this value and the groundwater endmember of $^{224}Ra$, the SGD can be calculated to support $^{224}Ra$ fluxes of $7.3\times10^9$ Bq/d (northern region) and of $14.42\times10^9$ Bq/d (southern region). Since it is difficult to evaluate the significance of this statement (this is the only relevant data published thus far), the $^{224}Ra/^{228}Th$ disequilibrium approach was not utilized in this study. However, comparable results of the $^{224}Ra/^{228}Th$ disequilibrium approach and SGD mass balance model demonstrate that the PEX most possibly represents an important component of benthic water exchange processes for short time scales in the HRE.

The utilization of the radium quartet as a proxy of SGD generally requires the construction of mass balances of the isotopes in the water column. Therefore, accurate constraints of all source terms and loss terms (other than SGD) are critically important. This is particularly the case in short-lived radium isotopes because of their rapid regeneration rates in bottom sediments. Compared with the traditional incubation method and the modeling approach (Beck et al., 2007; Garcia-Orellana et al., 2014; Rodellas et al., 2015), the $^{224}Ra/^{228}Th$ disequilibrium approach as pioneered by Cai et al. (2014, 2015, 2020) incorporates molecular diffusion, sediment mixing, and irrigation to estimate $^{224}Ra$ from benthic fluxes. A higher sampling resolution would be more helpful to constrain a $^{224}Ra$ based SGD budget in the estuary, where bottom sediments are generally highly heterogeneous and flow fields are very dynamic.

## 5 Conclusions

This study investigated the benthic biogeochemical characteristics of the HRE related to the influence of SGD. A SGD zonation was recognized and six subsections were defined accordingly. SGD fluxes in each zone were estimated and found to be very heterogeneous. The highest SGD flux was identified in the northwest nearshore zone, which was more than one order of magnitude higher than in the northwest offshore zone. Significant SGD resulted in low DO and pH, but elevated nutrient levels. The southeast nearshore zone was also characterized by a high SGD flux, but the bottom waters were more oxic because of the dominant inputs from the Huanghe River. Based on these observations, it can be speculated that a significant SGD may be an important contributor to the formation of coastal hypoxia and acidification. Although there are still unsolved pieces of the SGD puzzle and its associated ecological influence studies, which cause large uncertainties of all tracer source terms and final SGD flux results, the scientific communities has widely accepted SGD as an important source term for understanding the estuarine biogeochemical background.

***Acknowledgements***

We thank Yimin Zheng, Gang Xu and Zhenya Dou from the Qingdao Institute of Marine Geology, China Geological Survey for their assistance during the field observations and sample collection.

## References

Beck A J, Rapaglia J P, Cochran J K, et al. 2007. Radium mass-balance in Jamaica Bay, NY: Evidence for a substantial flux of submarine groundwater. Marine Chemistry, 106(3–4): 419-441

Burnett W C, Aggarwal P K, Aureli A, et al. 2006. Quantifying submarine groundwater discharge in the coastal zone via multiple methods. Science of the Total Environment, 367(2–3): 498–543

Burnett W C, Bokuniewicz H, Huettel M, et al. 2003. Groundwater and pore water inputs to the coastal zone. Biogeochemistry, 66(1): 3–33

Cai Pinghe, Shi Xiangming, Hong Qingquan, et al. 2015. Using $^{224}Ra/^{228}Th$ disequilibrium to quantify benthic fluxes of dissolved inorganic carbon and nutrients into the Pearl River Estuary. Geochimica et Cosmochimica Acta, 170: 188–203

Cai Pinghe, Shi Xiangming, Moore W S, et al. 2014. $^{224}Ra$: $^{228}Th$ disequilibrium in coastal sediments: Implications for solute transfer across the sediment–water interface. Geochimica et Cosmochimica Acta, 125: 68–84

Cai Pinghe, Wei Lin, Geibert W, et al. 2020. Carbon and nutrient export from intertidal sand systems elucidated by $^{224}Ra/^{228}Th$ disequilibria. Geochimica et Cosmochimica Acta, 274: 302–316

Charette M A, Sholkovitz E R. 2006. Trace element cycling in a subterranean estuary: part 2. Geochemistry of the pore water. Geochimica et Cosmochimica Acta, 70(4): 811–826

Cho H M, Kim G, Kwon E Y, et al. 2018. Radium tracing nutrient inputs through submarine groundwater discharge in the global ocean. Scientific Reports, 8(1): 2439, doi: 10.1038/s41598-018-20806-2

Garcia-Orellana J, Cochran J K, Bokuniewicz H, et al. 2014. Evaluation of $^{224}Ra$ as a tracer for submarine groundwater discharge in Long Island Sound (NY). Geochimica et Cosmochimica Acta, 141: 314–330

Guo Xiaoyi, Xu Bochao, Burnett W C, et al. 2020. Does submarine groundwater discharge contribute to summer hypoxia in the Changjiang (Yangtze) River Estuary?. Science of the Total Environment, 719: 137450, doi: 10.1016/j.scitotenv.2020.137450

Huettel M, Rusch A. 2000. Transport and degradation of phytoplankton in permeable sediment. Limnology and Oceanography, 45(3): 534–549

Kim G, Burnett W C, Dulaiova H, et al. 2001. Measurement of $^{224}Ra$ and $^{226}Ra$ activities in natural waters using a radon-in-air monitor. Environmental Science & Technology, 35(23): 4680–4683

Kroeger K D, Charette M A. 2008. Nitrogen biogeochemistry of submarine groundwater discharge. Limnology and Oceanography, 53(3): 1025–1039

Kwon E Y, Kim G, Primeau F, et al. 2014. Global estimate of submarine groundwater discharge based on an observationally constrained radium isotope model. Geophysical Research Letters, 41(23): 8438–8444

Liu Jianan, Du Jinzhou, Yi Lixin. 2017. Ra tracer-based study of submarine groundwater discharge and associated nutrient fluxes into the Bohai Sea, China: a highly human-affected marginal Sea. Journal of Geophysical Research: Oceans, 122(11): 8646–8660, doi: 10.1002/2017JC013095

Moore W S. 1996. Large groundwater inputs to coastal waters revealed by $^{226}Ra$ enrichments. Nature, 380(6575): 612–614

Moore W S. 2007. Seasonal distribution and flux of radium isotopes on the southeastern U. S. continental shelf. Journal of Geophysical Research: Oceans, 112(C10): C10013, doi: 10.1029/2007JC004199

Moore W S. 2010. The effect of submarine groundwater discharge on the ocean. Annual Review of Marine Science, 2: 59–88

Moore W S, Arnold R. 1996. Measurement of $^{223}Ra$ and $^{224}Ra$ in coastal waters using a delayed coincidence counter. Journal of

Geophysical Research: Oceans, 101(C1): 1321–1329
Moore W S, Blanton J O, Joye S B. 2006. Estimates of flushing times, submarine groundwater discharge, and nutrient fluxes to Okatee Estuary, South Carolina. Journal of Geophysical Research: Oceans, 111(C9): C09006, doi: 10.1029/2005JC003041
Moore W S, Sarmiento J L, Key R M. 2008. Submarine groundwater discharge revealed by $^{228}$Ra distribution in the upper Atlantic Ocean. Nature Geoscience, 1(5): 309–311, doi: 10.1038/ngeo183
Mulligan A E, Charette M A. 2006. Intercomparison of submarine groundwater discharge estimates from a sandy unconfined aquifer. Journal of Hydrology, 327(3–4): 411–425
Null K A, Corbett D R, DeMaster D J, et al. 2011. Porewater advection of ammonium into the Neuse River Estuary, North Carolina, USA. Estuarine, Coastal and Shelf Science, 95(2–3): 314–325
O'Connor A E, Krask J L, Canuel E A, et al. 2018. Seasonality of major redox constituents in a shallow subterranean estuary. Geochimica et Cosmochimica Acta, 224: 344–361
Peterson R N, Burnett W C, Taniguchi M, et al. 2008. Radon and radium isotope assessment of submarine groundwater discharge in the Yellow River delta, China. Journal of Geophysical Research: Oceans, 113(C9): C09021, doi: 10.1029/2008JC004776
Peterson R N, Moore W S, Chappel S L, et al. 2016. A new perspective on coastal hypoxia: the role of saline groundwater. Marine Chemistry, 179: 1–11
Qiu Hanxue, Zhen Xilai, Zhang Xiaolong, et al. 2003. Numerical analysis of groundwater discharge fluxes to ocean from the Huanghe farm area. Marine Geology Letters (in Chinese), 19(3): 28–33
Rao A M F, Polerecky L, Ionescu D, et al. 2012. The influence of porewater advection, benthic photosynthesis, and respiration on calcium carbonate dynamics in reef sands. Limnology and Oceanography, 57(3): 809–825
Rodellas V, Garcia-Orellana J, Masqué P, et al. 2015. Submarine groundwater discharge as a major source of nutrients to the Mediterranean Sea. Proceedings of the National Academy of Sciences, 112(13): 3926–3930
Rodellas V, Garcia-Orellana J, Trezzi G, et al. 2017. Using the radium quartet to quantify submarine groundwater discharge and porewater exchange. Geochimica et Cosmochimica Acta, 196: 58–73
Santos I R, Eyre B D. 2011. Radon tracing of groundwater discharge into an Australian estuary surrounded by coastal acid sulphate soils. Journal of Hydrology, 396(3–4): 246–257
Shi Xiangming, Benitez-Nelson C R, Cai Pinghe, et al. 2019. Development of a two-layer transport model in layered muddy-permeable marsh sediments using $^{224}$Ra–$^{228}$Th disequilibria. Limnology and Oceanography, 64(4): 1672–1687
Slomp C P, Van Cappellen P. 2004. Nutrient inputs to the coastal ocean through submarine groundwater discharge: controls and potential impact. Journal of Hydrology, 295(1–4): 64–86
Sun Yin, Torgersen T. 1998. The effects of water content and Mn-fiber surface conditions on $^{224}$Ra measurement by $^{220}$Rn emanation. Marine Chemistry, 62(3–4): 299–306
Swarzenski P W. 2007. U/Th series radionuclides as coastal groundwater tracers. Chemical Reviews, 107(2): 663–674
Taniguchi M, Ishitobi T, Chen Jianyao, et al. 2008. Submarine groundwater discharge from the Yellow River delta to the Bohai Sea, China. Journal of Geophysical Research: Oceans, 113(C6): C06025, doi: 10.1029/2007JC004498
Wang Xilong, Baskaran M, Su Kaijun, et al. 2018. The important role of submarine groundwater discharge (SGD) to derive nutrient fluxes into river dominated ocean margins-the East China Sea. Marine Chemistry, 204: 121–132
Wang Fenfen, Men Wu, Liu Guangshan. 2010. $^{226}$Ra and $^{228}$Ra in seawater of the north Yellow Sea. Journal of Oceanography in Taiwan Strait (in Chinese), 29(2): 265–276
Wang Xuejing, Li Hailong, Jiao J J, et al. 2015. Submarine fresh groundwater discharge into Laizhou Bay comparable to the Yellow River flux. Scientific Reports, 5: 8814, doi: 10.1038/srep08814
Wang Xuejing, Li Hailong, Luo Xin, et al. 2016. Using $^{224}$Ra to estimate eddy diffusivity and submarine groundwater discharge in Laizhou Bay, China. Journal of Radioanalytical and Nuclear Chemistry, 308(2): 403–411
Wang Xuejing, Li Hailong, Zhang Yan, et al. 2020. Investigation of submarine groundwater discharge and associated nutrient inputs into Laizhou Bay (China) using radium quartet. Marine Pollution Bulletin, 157: 111359
Waska H, Kim S, Kim G, et al. 2008. An efficient and simple method for measuring $^{226}$Ra using the scintillation cell in a delayed coincidence counting system (RaDeCC). Journal of Environmental Radioactivity, 99(12): 1859–1862
Xia Dong, Yu Zhigang, Xu Bochao, et al. 2016. Variations of hydrodynamics and submarine groundwater discharge in the Yellow River Estuary under the influence of the Water-Sediment Regulation Scheme. Estuaries and Coasts, 39(2): 333–343, doi: 10.1007/s12237-015-9994-7
Xu Bochao, Burnett W, Dimova N, et al. 2013. Hydrodynamics in the Yellow River Estuary via radium isotopes: ecological perspectives. Continental Shelf Research, 66: 19–28
Xu Bochao, Xia Dong, Burnett W C, et al. 2014. Natural $^{222}$Rn and $^{220}$Rn indicate the impact of the Water-Sediment Regulation Scheme (WSRS) on submarine groundwater discharge in the Yellow River Estuary, China. Applied Geochemistry, 51: 79–85
Xu Bocha, Yang Disong, Burnett W C, et al. 2016. Artificial water sediment regulation scheme influences morphology, hydrodynamics and nutrient behavior in the Yellow River Estuary. Journal of Hydrology, 539: 102–112
Yang Disong, Xu Bocha, Burnett W, et al. 2019. Radium isotopes-suspended sediment relationships in a muddy river. Chemosphere, 214: 250–258
Young C. 2013. Fate of nitrogen during submarine groundwater discharge into Long Island north shore embayments [dissertation]. New York, NY, USA: State University of New York at Stony Brook
Zhang Yan, Li Hailong, Guo Huaming, et al. 2020. Improvement of evaluation of water age and submarine groundwater discharge: A case study in Daya Bay, China. Journal of Hydrology, 586: 124775
Zhang Yan, Li Hailong, Wang Xuejing, et al. 2018. Submarine groundwater discharge and chemical behavior of tracers in Laizhou Bay, China. Journal of Environmental Radioactivity, 189: 182–190

# Supplementary information:

**Table S1**. The activities of $^{223}$Ra, $^{224}$Ra and $^{226}$Ra in the surface seawater and bottom seawater of the Huanghe River Estuary

**Table S2**. Depth (m), pH, temperature (°C), salinity, DO (mg/L), turbidity (FTU), DIP (mol/L), DIN (mol/L), DSi (mol/L) of bottom water at sample sites for the Huanghe River Estuary

**Table S3**. Zonation, pH, temperature (°C), salinity, DO (mg/L), turbidity (FTU), DIP (mol/L), DIN (mol/L), DSi (mol/L) of surface water at sample sites for the Huanghe River Estuary

The supplementary information is available online at https://doi.org/10.1007/s13131-021-1882-3 and http://www.aosocean.com/. The supplementary information is published as submitted, without typesetting or editing. The responsibility for scientific accuracy and content remains entirely with the authors.